ADVANCED FUNCTIONAL MATERIALS
www.afm-journal.de

Comparative Studies on Optical, Redox, and Photovoltaic Properties of a Series of D–A–D and Analogous D–A Chromophores

André Zitzler-Kunkel, Martin R. Lenze, Tobias Schnier, Klaus Meerholz, and Frank Würthner**

A series of new symmetrical donor-acceptor-donor (D–A–D) dyes based on *s*-indacene-1,3,5,7(2*H*,6*H*)-tetraone as an acceptor unit containing varying electron donating moieties and analogous donor-acceptor (D–A) chromophores with indane-1,3-dione as an acceptor are synthesized. By employing these two sets of dyes, the influence of a scaffold change from unsymmetric push-pull (D–A) to symmetrical (D–A–D) systems on optical, electrochemical, and photovoltaic properties are explored. Detailed comparative studies reveal favorable optical characteristics and considerably decreased bandgaps for the D–A–D dyes compared to those of the reference D–A chromophores. Accordingly, the evaluation of the present dyes as donor materials in bulk heterojunction (BHJ) solar cells in combination with fullerene derivatives $PC_{61}BM$ or $PC_{71}BM$ as acceptors afforded significantly improved performance for devices based on D–A–D blends (up to a factor of 4 compared to the respective D-A reference) with power conversion efficiencies of up to 2.8%. In less polar solvents such as toluene, some of the novel D–A–D chromophores exhibit unexpectedly high fluorescence quantum yields Φ_{em} of up to unity, in striking contrast to their weakly fluorescent D-A counterparts.

1. Introduction

Over the past decade π-conjugated low band gap organic molecules have gained a great deal of attention as highly attractive organic electronic materials.[1] In the field of organic photovoltaics, which is a prominent sector of organic electronic materials, immense research efforts have been devoted to the design of new co-polymers with $(–D–A–)_n$ backbone based on such π-conjugated molecules comprising alternating electron-rich (donor D) and electron-deficient (acceptor A) units.[2] The use of tailored state-of-the-art narrow band gap polymeric donors in combination with the soluble fullerene derivative [6,6]-phenyl-C_{71}-butyric acid methyl ester ($PC_{71}BM$) in a bulk heterojunction (BHJ)[3] architecture afforded organic solar cells (OSC) reaching power conversion efficiencies (PCE) exceeding 9%.[4] Although in this regard conjugated small molecule-based OSCs[5] still lag behind their polymeric counterparts, the simple synthesis and purification, monodispersity, tunability of optical and electronic as well as solubility properties, and potential vacuum processibility have stimulated intense research efforts in the development of small molecule materials. However, in contrast to polymeric semiconductors with alternating $(–D–A–)_n$ framework, for small molecules the question arises how to properly combine the donor and acceptor subunits in the molecular scaffold to achieve desired material properties.

Indeed, in the recent years the search for new small molecule-based donor systems resulted in the development of a large variety of promising organic materials with different donor-acceptor subunit combinations. For example, symmetrical acceptor-donor-acceptor (A–D–A)[6] and few donor-acceptor-donor (D–A–D),[6a,7] sophisticated A–D–A´–D–A[8] and D–A–D´–A–D,[9] as well as unsymmetrical D–A[10] and D–A–A´[11] systems have been achieved with PCEs approaching those of polymeric pendants. For such photovoltaic materials the use of prominent chemical frameworks, e.g. oligothiophene,[6b–d,8] triarylamine,[7b,c,11,12] diketopyrrolopyrrole,[7a] BODIPY,[13] isoindigo[6a] as well as squaraine,[14] and more recently dithienosilole[9] and benzodithiophene[6e] structural units have been reported.

The use of above-mentioned electron donating and accepting groups in molecular semiconductors evokes an effective internal charge transfer and leads to increased conjugation along the molecular π-scaffold, imparting the desired broad absorption profiles and narrow band gaps. In principle, these desired optical and electronic features could be achieved by application of simple D–A (push-pull) chromophores such as merocyanines.[15] Along this line our particular interest in the last few years has been devoted to the design of merocyanines with tailored HOMO/LUMO levels, which we could place among the top-performing small molecule donor materials[10]

A. Zitzler-Kunkel, Prof. F. Würthner
Institut für Organische Chemie &
Center for Nanosystems Chemistry
Universität Würzburg
Am Hubland 97074, Würzburg, Germany
E-mail: wuerthner@chemie.uni-wuerzburg.de
M. R. Lenze, T. Schnier, Prof. K. Meerholz
Universität zu Köln
Department of Chemistry
Luxemburger Straße 116, 50939, Köln, Germany
E-mail: klaus.meerholz@uni-koeln.de

DOI: 10.1002/adfm.201400455

© 2014 WILEY-VCH Verlag GmbH & Co. KGaA, Weinheim

despite their inherent dipolarity, which is considered to hamper the charge carrier transport according to the Bässler model.[16] The rather unexpected high performance of merocyanine donor materials in OSCs could be rationalized in terms of the formation of centrosymmetric dimers[17] with canceled out dipole moments on the supramolecular and device level.[18]

We anticipate that the alteration of the molecular backbone of merocyanine from a D–A (push-pull) to symmetrical D–A–D scaffold would give rise to a significant loss of inherent dipolarity on the molecular level and an expansion of the π-conjugation. Both aspects are considered to be advantageous for material properties.

Remarkably, there is an apparent lack of comparative studies of D–A–D and analogous D–A systems exploring the influence of scaffold alteration on molecular and photovoltaic properties. Moreover, only few symmetrical D–A–D dyes with semiconducting properties have been reported to date.[6a,7] Thus, we have synthesized a series of new symmetrical D–A–D chromophores **1–3** based on *s*-indacene-1,3,5,7(2*H*,6*H*)-tetraone as central acceptor unit and analogous unsymmetrical D–A dyes **4–6** (for structures, see **Scheme 1**) with indane-1,3-dione as acceptor, and investigated their optical, electrochemical and photovoltaic properties. Our comparative studies with these two sets of compounds indeed reveal a substantial, up to four-fold increase of the PCE values for solution-processed D–A–D:PCBM (i.e. $PC_{61}BM$ and $PC_{71}BM$) devices compared to those of D–A analogues. By thorough optimization of D–A–D donor based devices a PCE as high as 2.8% could be achieved.

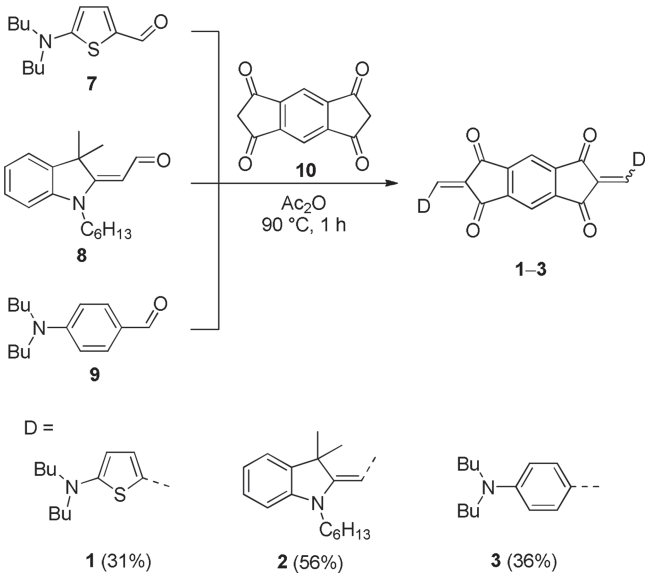

Scheme 2. Synthetic route to tetraone dyes **1–3**.

2. Results and Discussion

2.1. Synthesis

The D–A–D dyes **1–3** (further denoted as tetraone dyes) with central indacene-1,3,5,7-tetraone electron accepting unit were synthesized by a Knoevenagel condensation reaction of CH-acidic indacene derivative **10**[19] with the respective aldehyde-functionalized electron-rich building blocks **7–9** in 31 to 56% yields (**Scheme 2**). The reference D–A chromophores **4**,[20] and **6**[21] are literature known, while **5** was synthesized according to the procedure[22] reported for an analogous compound. The new tetraone dyes **1–3** were characterized by common spectroscopic and analytical techniques. They were obtained as a 1:1 mixture of *cis* and *trans* isomers as revealed by NMR spectroscopy (for details see the Supporting Information, Figure S1 and S2). The detailed synthetic procedures and characterization data are reported in the Experimental Section.

2.2. Optical Properties

The absorption and emission characteristics of the dyes **1–6** have been investigated by UV–vis and fluorescence spectroscopy. The UV–vis spectra in dilute dioxane solution (c = 10^{-5} M) are displayed in **Figure 1**, and the significant optical properties are summarized in **Table 1**. The D–A–D compounds **1** and **2** bearing aminothiophene and indoline as donor moieties, respectively, exhibit a comparatively sharp, intense,

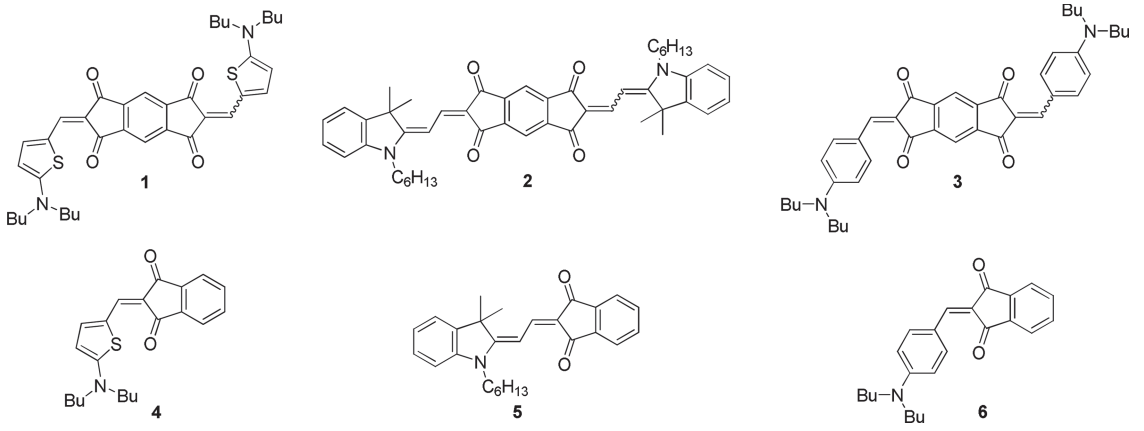

Scheme 1. Chemical structures of D–A–D (**1–3**) and D–A (**4–6**) molecules studied in this work.

© 2014 WILEY-VCH Verlag GmbH & Co. KGaA, Weinheim

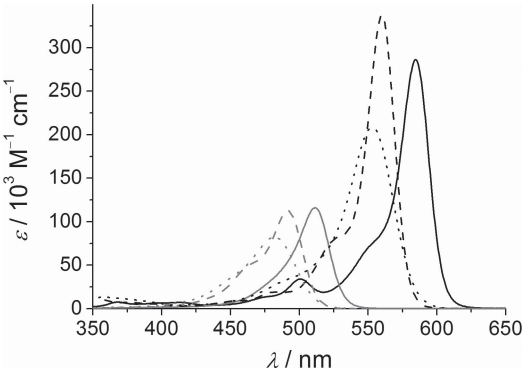

Figure 1. UV–vis absorption spectra of the D–A–D dyes **1** (black solid line), **2** (black dashed line), **3** (black dotted line) and the respective D–A dyes **4** (grey solid line), **5** (grey dashed line) and **6** (grey dotted line) in dioxane ($c = 1 \times 10^{-5}$ M at 25 °C).

cyanine-like absorption band culminating at 585 nm and 561 nm, respectively, with an additional vibronic shoulder at shorter wavelengths, while the phenylamine-containing dye **3** shows a broader absorption profile without vibronic fine structure, exhibiting an absorption maximum at $\lambda_{max} = 553$ nm. Similar spectroscopic changes were observed for the corresponding D–A chromophores **4–6** containing the same donor units. Notably, a substantial red-shift (70–85 nm) of the absorption maxima is observed for the tetraone dyes **1–3** compared with the respective push-pull dyes **4–6**, which might be explained by the increased conjugation length in the D–A–D structures.[23] Moreover, the tetraone chromophores exhibit significantly higher (2–3 fold) molecular absorption coefficients compared to those of the corresponding D–A dyes at the absorption maximum reaching values of up to $\varepsilon = 3.4 \times 10^5$ M^{-1} cm^{-1} for **2**.

Since the absorption strength of a dye is strongly dependent on its molar mass and the broadness of its absorption profile, we have determined the absorption density μ^2_{ag} M^{-1}[10b] of these dyes (μ_{ag} = transition dipole moment) which is directly related to the chromophores tinctorial strength (see Table 1). Indeed, the increased conjugation length in the molecular scaffold of tetraone dyes resulted in a considerable increase of their absorption densities (10% for **1** and 22% for **2** and **3**, respectively) compared to those of the respective D–A chromophores **4**, **5** and **6**.

Next, we have studied the fluorescence properties of the present series of chromophores in dioxane.[26] The push-pull dyes **4** and **6** are nonfluorescent (fluorescence quantum yield $\Phi_{em} < 0.001$) in this solvent, while the indoline-donor-based dye **5** shows weak green light emission with a quantum yield of $\Phi_{em} = 0.03$. Notably, the scaffold transformation from the unsymmetric D-A to the symmetrical D–A–D systems results in a significant enhancement of Φ_{em} by more than one order of magnitude, reaching $\Phi_{em} = 0.06$ for **1**, $\Phi_{em} = 0.30$ for **3**, and even up to $\Phi_{em} = 0.90$ for **2**. Similar effect has previously been reported for triphenylamine-thienylenevinylene hybrid systems.[27] Moreover, the symmetric tetraone dyes **1–3** show smaller Stokes shifts than the unsymmetric respective counterparts **4–6** (Table 1), suggesting a rigidification of the D–A–D chromophore backbone that impedes conformational changes and vibronic coupling between ground and first excited state and hence attaining increased tinctorial strength and emission properties of the D–A–D chromophores.

To acquire more insight into the strikingly different emission behavior of the tetraone dyes compared to that of D–A references, we have performed further experiments by steady-state and time-resolved fluorescence spectroscopy for the most fluorescent tetraone dye **2** and its push-pull analogue **5** in solvents of different polarity. The data shown in **Table 2** reveal that the fluorescence quantum yield of tetraone **2** is strongly influenced by the permittivity (ε_r) of the solvent. In solvents of low polarity such as toluene and dioxane (ε_r = 2.38 and ε_r = 2.21, respectively) it exhibits quantum yields of almost unity ($\Phi_{em} \approx 1.00$ in toluene and $\Phi_{em} = 0.90$ in dioxane). However, with increasing permittivity of the solvents Φ_{em} decreases significantly, and finally in the highly polar DMF (ε_r = 36.71) dye **2** is essentially nonfluorescent (Table 2). In agreement with the quantum yields, the fluorescence lifetime (τ_{em}) of tetraone **2** decreases from 1.8 ns in the nonpolar toluene to below the system's resolution (<0.5 ns) in solvents of higher polarity. We calculated the radiative and nonradiative rate constants k_r and k_{nr} from Φ_{em} and τ_{em} (see Table 2). While k_r is essentially constant in all solvents studied here, k_{nr} increases with increasing solvent polarity by two orders of magnitude. Thus, the decrease of Φ_{em} with increasing solvent polarity originates from the enhancement of k_{nr} which indicates a fluorescence quenching pathway via a charge transfer state that is energetically favored by polar environments.[28]

In striking contrast to tetraone dye **2**, the fluorescence quantum yield of the respective dione acceptor based D–A dye

Table 1. Optical properties of the investigated chromophores **1–6** in dioxane.

Dye	λ_{max} [nm]	ε_{max} [M^{-1} cm^{-1}]	$\mu^2_{ag}/M^{a)}$ [D^2 mol/g]	λ_{em} [nm]	Φ_{em}	Δ_{Stokes} [nm]
1[b)]	585	286000	0.24	596	0.06[d)]	11
4[c)]	512	116000	0.22	548	<0.001	36
2[b)]	561	337000	0.27	571	0.90[e)]	10
5[c)]	492	113000	0.22	511	0.03[d)]	19
3[b)]	553	209000	0.28	582	0.30[d)]	29
6[c)]	482	82000	0.23	529	<0.001	47

[a)]For the determination of the transition dipole moment μ_{ag} by integration of $\varepsilon(\tilde{\nu})$, see the Supporting Information; [b)]Fluorescence standard: *N,N'*-di(2,6-diisopropylphenyl)-1,6,7,12-tetraphenoxyperylene-3,4:9,10-tetracarboxylic acid bisimide in chloroform; $\Phi_{em} = 0.96$;[24] [c)]Fluorescence standard: *N,N'*-di(2,6-diisopropylphenyl)-perylene-3,4:9,10-tetracarboxylic acid bisimide in chloroform; $\Phi_{em} = 1$;[25] [d)]$\Phi_{em} \pm 0.01$; [e)]$\Phi_{em} \pm 0.03$.

© 2014 WILEY-VCH Verlag GmbH & Co. KGaA, Weinheim

Table 2. Solvent dependent absorption and emission properties of D–A–D dye **2**.

Solvent (ε_r)[a)]	λ_{max} [nm]	λ_{em} [nm]	Δ_{Stokes} [nm]	Φ_{em}	τ_{em} [ns][b)]	k_r [s^{-1}][c)]	k_{nr} [s^{-1}][d)]
Dioxane (2.21)	561	571	10	0.90[e)]	1.3	7.1×10^8	6.1×10^7
Toluene (2.38)	561	572	11	≈1.00[f)]	1.8	5.6×10^8	$\leq 5.6 \times 10^{6}$[h)]
$CHCl_3$ (4.89)	572	584	12	0.20[e)]	0.6	3.3×10^8	1.3×10^9
THF (7.58)	566	578	12	0.37[g)]	0.7	5.3×10^8	9.0×10^8
CH_2Cl_2 (8.93)	573	584	11	0.08[f)]	<0.5	$>1.6 \times 10^8$	$>1.3 \times 10^9$
DMF (36.71)	575	—	—	≈0.00[f)]	<0.5	$\geq 2.0 \times 10^{7}$[i)]	$\geq 2.0 \times 10^{9}$[i)]

[a)]The permittivity values (ε_r) of the solvents are taken from ref [30]; [b)] $\tau_{em} \pm 0.2$ ns; [c)] $k_r = \Phi_{em} \cdot \tau_{em}^{-1}$; [d)] $k_{nr} = (1-\Phi_{em}) \cdot \tau_{em}^{-1}$; [e)] $\Phi_{em} \pm 0.03$; [f)] $\Phi_{em} \pm 0.01$; [g)] $\Phi_{em} \pm 0.02$; [h)]Value calculated using $\Phi_{em} \geq 0.99$; [i)]Value calculated using $\Phi_{em} \leq 0.01$.

5 is almost independent of the solvent polarity with Φ_{em} values of around 0.04 in all applied solvents (see Table S1 in the Supporting Information). Accordingly, this dye shows solvent-independent fluorescence lifetimes below 0.5 ns, impeding the calculation of the k_r and k_{nr} values. The low fluorescence quantum yield of molecule **5**, even in less polar solvents, is in accordance with those measured for many other D–A dyes.[29] In general it is assumed for this class of dyes that torsional vibrations and/or rotations around the C–C bonds of the polymethine chain are responsible for the quenched fluorescence. Nevertheless, the strikingly different fluorescence properties of D–A–D dye **2** raise doubts about this interpretation and motivate further studies by time-resolved spectroscopy. Although the smaller Stokes shift and the more cyanine-like spectral shape of D–A–D dye **2** may be taken as evidence for a reduced conformational flexibility and accordingly higher rigidity of D–A–D dye **2** compared to D–A dye **5**.

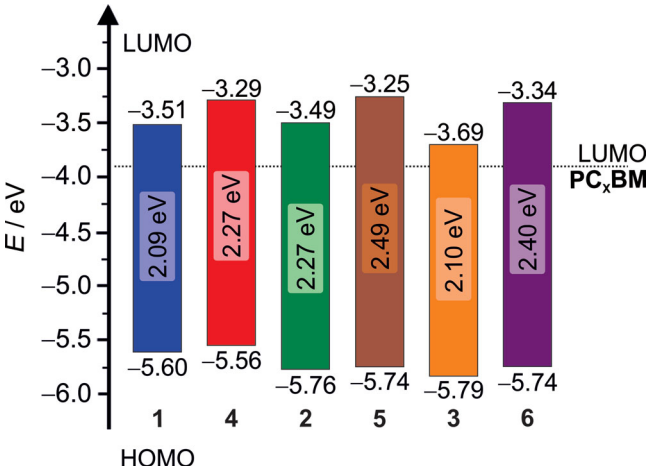

Figure 2. FMO energy levels and band gap (solid area) of dyes **1–6** and their relative position to the LUMO of $PC_{61}BM$.

2.3. Electrochemistry and Energy Levels

Cyclic voltammetry (CV) measurements were performed in dichloromethane/NBu_4PF_6 using Fc/Fc^+ redox couple as an internal standard to determine the oxidation and reduction potentials of the dyes **1–6**. The data were transformed into frontier molecular orbital (FMO) energy levels vs. vacuum (see **Figure 2**)[31] and compared to the optical gap calculated from the absorption wavelength, yielding reasonably good agreement (see Table S2 in the Supporting Information).

Similar electron donor strength of indoline-dimethine and aminophenyl moieties in compounds **5** and **6** is reflected in their identical HOMO energies of –5.74 eV vs. vacuum. In contrast, the increased electron donating propensity of the amino-thienyl unit in dye **4** results in an increase of the HOMO energy by ca. 0.2 eV compared to that of **5** and **6**, respectively. The LUMO energies are very similar in all three dyes **4–6**, indicating negligible influence of the donor moieties.

In the D–A–D dyes **1–3** the HOMO energy barely varies compared to the respective D–A counterparts **4–6**, thus the predominant contribution to the reduction of the optical gap comes from a reduction of the LUMO level (by 0.33 – 0.42 eV) due to the introduction of a stronger central acceptor unit. In view of photovoltaic properties, the lower-lying LUMO levels of D–A–D dyes should not be disadvantageous since the remaining offset relative to the LUMO level of the used fullerene acceptors (–3.91 eV)[32] still constitutes a sufficient driving force for charge carrier separation.[1a]

2.4. DFT Calculations

Quantum chemical DFT calculations were performed to gain further insights into the effect of scaffold change on the electronic properties of the molecules. In **Figure 3** the electron density distributions of the HOMO and LUMO of the chromophore pair **3** and **6** are shown as an example (for all other computed structures see Figure S11 in the Supporting Information). The electron densities of the HOMOs of both D–A–D and D–A systems are predominantly localized on the donor moiety, releasing the HOMO energy independent of the applied acceptor unit. Furthermore, it is obvious from Figure 3 that the central part of the tetraone is barely involved in the HOMO, i.e. the dye appears to be composed of two independent merocyanine subunits. Accordingly, this analysis provides a rationale for the almost identical HOMO levels (Figure 2) of the respective D–A–D/ D–A pairs **1**/**4**, **2**/**5** and **3**/**6**. In contrast, the electron densities of the LUMOs are distributed over the entire molecule. In view of this finding, the enlarged scaffold of

© 2014 WILEY-VCH Verlag GmbH & Co. KGaA, Weinheim

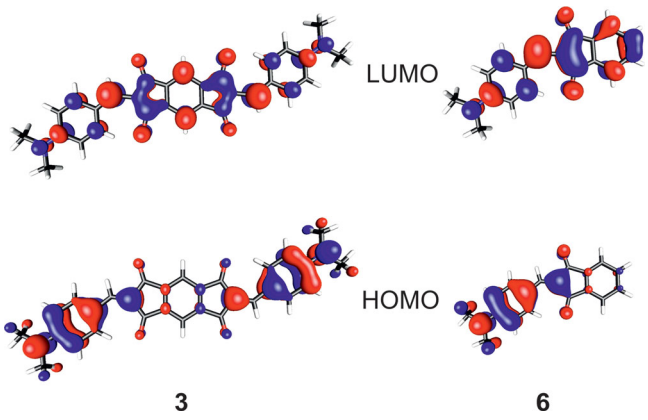

Figure 3. HOMO and LUMO electron density distribution (Turbomole V5.10; RIDFT/ B3LYP; basis sets: TZVP/TZV) of dyes **3** (left) and **6** (right). For simplicity, butyl chains are replaced by methyl groups.

tetraone compared with push-pull chromophores should lead to an extension of the conjugation length and hence a shift of the LUMO level to lower energies, which was indeed observed (see Figure 2). Thus, the DFT calculations are in accordance with the experimental results and confirm the effect of scaffold modification on the frontier molecular orbital energies.

2.5. BHJ Solar Cells

Finally, the impact of scaffold change from D–A to D–A–D systems on the photovoltaic performance has been investigated by using the dyes **1–6** as donor materials in solution-processed BHJ solar cells. For these studies, the D–A–D compounds **1–3** were used as a 1:1 mixture of *cis* and *trans* isomers as obtained by the respective synthesis. Employing two different fullerene acceptors, $PC_{61}BM$ and $PC_{71}BM$, and two different hole-collecting contacts (HCC), PEDOT:PSS and molybdenum oxide (MoO_3), afforded four series of OSC. The general device architecture was glass/ITO/HCC/active layer/Ca/Ag. Details about device fabrication and characterization are provided in the Experimental Section. The fabricated solar cells were optimized regarding the active layer thickness and dye:fullerene ratio. An active layer thickness of about 50 nm with fullerene content of approximately 70 wt% was found to produce best devices, except for dye **1** that exhibited better efficiency at a lower fullerene content (50 wt%, see Figure S20 and S21 in the Supporting Information).

The characteristic solar-cell parameters of the four device series are compiled in **Table 3**. In agreement with earlier results, the use of MoO_3 as HCC instead of PEDOT:PSS generally leads to an increase of the open-circuit voltage (V_{OC}), accompanied by

Table 3. Characteristic solar cell parameters for devices glass/ITO/HCC/dye **1–6**:PC_XBM/Ca/Ag under simulated AM1.5G illumination intensity of 100 mW cm^{-2}.

Dye	wt% PC_XBM	HCC	V_{OC} [V]	J_{SC} [mA cm^{-2}]	*FF*	PCE [%]
1	50 (X = 61)	PEDOT:PSS	0.69	5.14	0.36	1.28
4	70 (X = 61)	PEDOT:PSS	0.61	2.36	0.32	0.45
2	70 (X = 61)	PEDOT:PSS	0.68	5.32	0.35	1.27
5	70 (X = 61)	PEDOT:PSS	0.67	2.16	0.29	0.41
3	75 (X = 61)	PEDOT:PSS	0.64	3.62	0.57	1.32
6	70 (X = 61)	PEDOT:PSS	0.53	2.13	0.26	0.29
1	50 (X = 61)	MoO_3	0.83	5.61	0.47	2.21
4	70 (X = 61)	MoO_3	0.74	2.50	0.36	0.66
2	70 (X = 61)	MoO_3	0.95	5.75	0.42	2.30
5	70 (X = 61)	MoO_3	0.75	2.50	0.32	0.60
3	75 (X = 61)	MoO_3	0.89	3.16	0.67	1.87
6	70 (X = 61)	MoO_3	0.83	2.96	0.34	0.85
1	50 (X = 71)	PEDOT:PSS	0.71	5.72	0.37	1.49
4	70 (X = 71)	PEDOT:PSS	0.63	3.61	0.30	0.69
2	70 (X = 71)	PEDOT:PSS	0.67	6.09	0.33	1.35
5	70 (X = 71)	PEDOT:PSS	0.68	2.82	0.28	0.54
3	75 (X = 71)	PEDOT:PSS	0.34	2.39	0.31	0.25
6	70 (X = 71)	PEDOT:PSS	0.54	2.51	0.24	0.33
1	50 (X = 71)	MoO_3	0.84	6.39	0.49	2.61
4	70 (X = 71)	MoO_3	0.74	4.00	0.39	1.15
2	70 (X = 71)	MoO_3	0.94	7.16	0.41	2.81
5	70 (X = 71)	MoO_3	0.77	3.41	0.32	0.83
3	75 (X = 71)	MoO_3	0.28	2.75	0.28	0.22
6	70 (X = 71)	MoO_3	0.80	3.82	0.33	1.00

© 2014 WILEY-VCH Verlag GmbH & Co. KGaA, Weinheim

an increase of the fill factor (*FF*), while the short-circuit current (J_{SC}) varies non-systematically; these findings are commonly attributed to the more favorable energy level alignment of the low-lying HOMO level of the dyes with the high work function metal oxide[33] and a reduced contact resistance.[33] Similarly, the use of $PC_{71}BM$ instead of $PC_{61}BM$ as acceptor in the active layer generally leads to an increase of J_{SC} while V_{OC} and *FF* are little affected; this is commonly attributed to the higher absorption coefficient of $PC_{71}BM$.[32]

Devices based on the new tetraone dyes **1–3** are consistently more efficient by a factor of 2–4 than those based on the reference dyes **4–6** (an exception is dye **3** in combination with the fullerene $PC_{71}BM$, which will be discussed separately below). This improvement of the photovoltaic performance results from the strong increase of *FF* and J_{SC}, which can be ascribed to the following aspects:

(i) The absorption of dyes **1–3** is considerably higher compared to that of reference compounds **4–6** (compare Table 1).
(ii) The bathochromic shift of the absorption in **1–3** results in a better spectral overlap with the solar spectrum and thus enhances harvesting of solar photons.
(iii) Due to the reduced dipolar character of **1–3**, the charge carrier mobilities of electrons and holes in devices based on these donor materials should be more balanced.
(iv) The dyes **1–3** generally show improved film forming properties as compared to the references **4–6**. As a result, the fill factors *FF* are slightly increased. Devices based on **3**:$PC_{61}BM$ exhibit an outstanding *FF* of 0.57 and even 0.67 on PEDOT:PSS and MoO_3 as HCC, respectively, due to a more favorable active layer morphology. Unfortunately, in the case of **3**:$PC_{71}BM$ coarse separation of the phases dramatically reduces the device performance (see Figure S22 in the Supporting Information).

The *J–V* characteristics of the optimized BHJ solar cells with dyes **1–6** are depicted in **Figure 4**a and c. For the optimized device with dye **1** as donor significantly improved PCE of 2.61% was observed (compared to 1.15% for the reference compound **4**; Table 3). Dye **2** exhibited even better performance with a PCE of 2.81% (compared to 0.83% for the reference compound **5**). For dye **3** V_{OC} and *FF* were improved to 0.89 V and 0.67, respectively, but accompanied by a reduction of J_{SC} to 3.16 mA cm^{-2} leading to a power conversion efficiency of only 1.87% (compared to 0.85% for the reference compound **6** under identical conditions).

The external quantum efficiency (*EQE*) spectra of solar cells based on dyes **1–6** are shown in Figure 4b and d. Devices with **1** and **2** exhibit appreciable photoconversion efficiency in the spectral range from 350 to 680 (**1**) and 650 nm (**2**), respectively, with two maxima of 30% at 380 nm and 49% at 630 nm for **1** and 38% at 370 nm and 56% at 590 nm for **2**, reflecting the dye absorption in the thin films (Figure 1). Due to the absence of

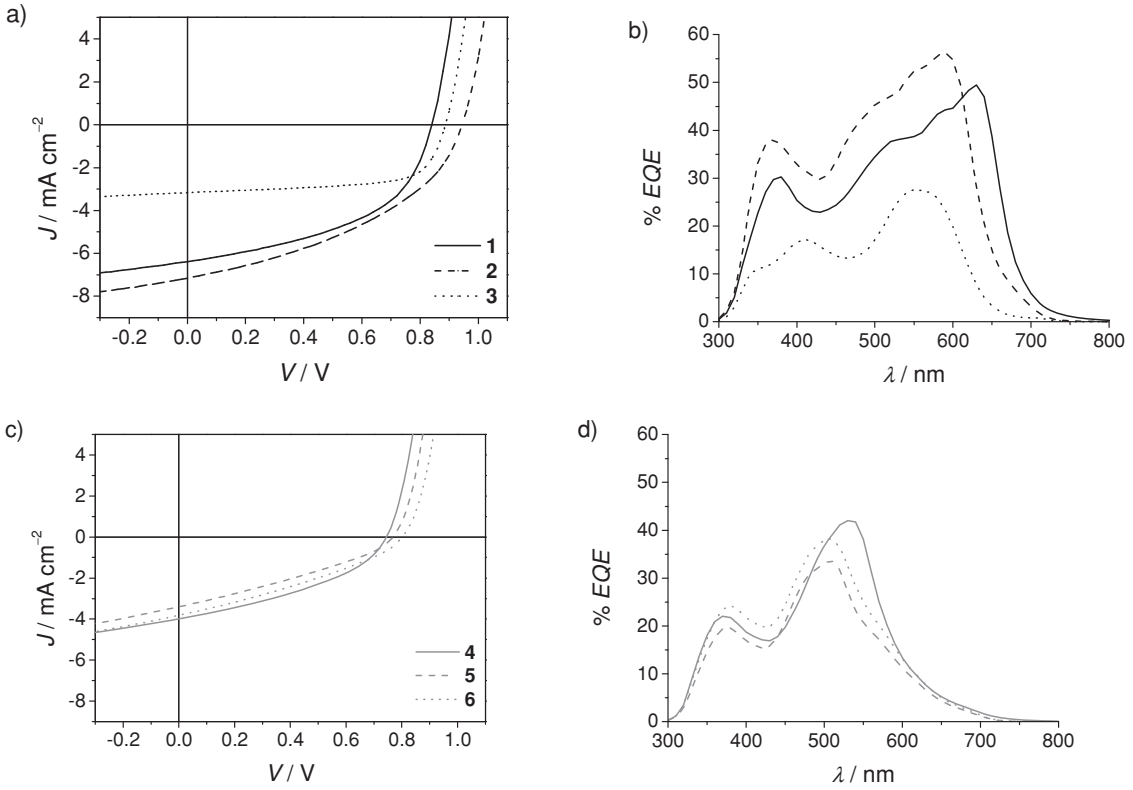

Figure 4. (a,c) *J–V* response and (b,d) *EQE* spectra of optimized BHJ solar cell devices based on D–A–D dyes **1–3** (a,b) and reference D–A dyes **4–6** (c,d) measured under simulated AM1.5G solar illumination (100 mW cm^{-2}): **1** (black solid line, 50 wt% $PC_{71}BM$), **2** (black dashed line, 70 wt% $PC_{71}BM$), **3** (black dotted line, 75 wt% $PC_{61}BM$), **4** (grey solid line, 70 wt% $PC_{71}BM$), **5** (grey dashed line, 70 wt% $PC_{71}BM$) and **6** (grey dotted line, 70 wt% $PC_{71}BM$).

© 2014 WILEY-VCH Verlag GmbH & Co. KGaA, Weinheim

$PC_{71}BM$ and the inherently lower J_{SC} with $PC_{61}BM$, the optimized device with **3** reveals rather low quantum efficiency with a maximum of 28% at 550 nm.

3. Conclusion

The molecular properties (optical, electronic) of symmetrical D–A–D chromophores **1–3** with indacene-1,3,5,7-tetraone as electron accepting central unit markedly differ from those of analogous D–A dyes **4–6**. The tetraones **1–3** exhibit ca. 80 nm red-shifted, sharp absorption bands with increased tinctorial strength compared to those of references **4–6**. Therefore, these dyes exhibit some similarity with more common cyanine and squaraine dyes. To our surprise, these D–A–D dyes feature distinctly enhanced photoluminescence properties in nonpolar solvents which warrants further investigations. The LUMO delocalization over the whole molecule of tetraone chromophores leads to ca. 0.3 eV shift to lower energies compared to the LUMO levels of the reference push-pull chromophores, whereas the HOMO levels remained almost unchanged compared to their D–A counterparts. According to this, it is interesting to consider the arising properties of $(–D–A–)_n$ polymers composed of tetraone acceptor units. In such polymers the LUMO should be much more delocalized than the HOMO which might lead to n-type semiconducting polymers, which are still very rare compared to their p-type counterparts. BHJ solar cells with D–A and D–A–D donors show little effect on the V_{OC} but a strong increase of J_{SC} and *FF* for D–A–D dyes due to their extended absorption to the NIR region, leading to up to four-fold increase of the PCE for D–A–D:PCBM blends. The optimized solar cells based on D–A–D donors afforded PCE as high as 2.81%. Our detailed comparative investigations reveal that the molecular scaffold change from push-pull to symmetrical donor-acceptor-donor system is a promising concept to improve the material properties for luminescence and photovoltaic applications.

4. Experimental Section

Materials and Methods: All solvents and reagents were purchased from commercial sources and used as received without further purification, unless otherwise stated. Column chromatography was performed using silica gel 60M (0.04–0.063 mm) from Macherey-Nagel. ^{1}H and ^{13}C NMR spectra were recorded on Bruker Advance 400 or Bruker Advance DMX 600 and calibrated to the residual solvent peak. All chemical shifts δ are in ppm. High-resolution mass spectra (ESI) were recorded on an ESI MicrOTOF Focus spectrometer from Bruker Daltonics. Elemental analyses were performed on a CHNS 932 analyzer (Leco Instruments GmbH, Mönchengladbach, Germany).

Synthesis of ***1***: D–A–D dye **1** was synthesized by stirring a mixture of *s*-indacene-1,3,5,7(2*H*,6*H*)-tetraone (200 mg, 0.93 mmol) and 5-(dibutylamino)thiophene-2-carbaldehyde (**7**; 447 mg, 1.86 mmol) in acetic anhydride (2 mL) at 90 °C for 30 min. After cooling down to room temperature, 2-propanol and *n*-hexane were added to the mixture. The precipitated solid was collected by suction and washed successively with 2-propanol, toluene and *n*-hexane. The crude product was purified by column chromatography (silica, DCM/MeOH 100:2). After precipitation from DCM solution by adding 2-propanol/*n*-hexane (1:4) and drying in vacuum the pure product was obtained in 31% yield (189 mg, 0.29 mmol) as a red solid; Mp. 253–254 °C; ^{1}H NMR (CD_2Cl_2, 400 MHz, δ): 7.95 (s, 2H), 7.70 (s, 2H), 7.62 (d, J = 4.8 Hz, 2H), 6.28 (d, J = 4.8 Hz, 2H), 3.53 (t, J = 7.8 Hz, 8H), 1.79–1.70 (m, 8H), 1.49–1.38 (m, 8H), 1.00 (t, J = 7.4 Hz, 12H); ^{13}C NMR (CD_2Cl_2, 101 MHz, δ): 190.1, 190.0, 189.1, 189.0, 173.8, 150.4, 146.5, 146.3, 145.4, 145.2, 136.1, 123.5, 115.0, 114.2, 114.0, 113.8, 109.2, 54.3, 29.7, 20.6, 14.0; UV–vis (CH_2Cl_2): λ_{max} (ε) = 598 nm (280000 M^{-1} cm^{-1}); HRMS (ESI) *m/z*: $[M]^+$ calcd for $C_{38}H_{44}N_2O_4S_2$, 656.2737; found, 656.2734; Anal. calcd for $C_{38}H_{44}N_2O_4S_2{\cdot}0.5\ H_2O$: C 68.54, H 6.81, N 4.21, S 9.63; found: C 68.42, H 6.85, N 4.22, S 9.47.

Synthesis of ***2***: This dye was synthesized using (*E*)-2-(1-hexyl-3,3-dimethylindolin-2-ylidene)acetaldehyde (**8**) as a starting material according to the same procedure described above for compound **1**. Yield: 403 mg (0.56 mmol, 56%), red solid; Mp. 326–328 °C; ^{1}H NMR (CD_2Cl_2, 600 MHz, δ): 8.13 (d, J = 14.2 Hz, 2H), 8.02–7.96 (m, 2H), 7.56 (d, J = 14.3 Hz, 2H), 7.40–7.33 (m, 4H), 7.23–7.17 (m, 2H), 7.07 (d, J = 7.9 Hz, 2H), 4.01 (t, J = 7.5 Hz, 4H), 1.92–1.82 (m, 4H), 1.74 (s, 12H), 1.55–1.32 (m, 12H), 0.91 (t, J = 7.1 Hz, 6H); ^{13}C NMR (CD_2Cl_2, 151 MHz, δ): 190.6, 190.6, 189.8, 189.7, 175.6, 146.7, 146.4, 145.1, 144.8, 142.7, 142.3, 141.4, 128.5, 124.6, 122.4, 117.1, 114.3, 113.9, 113.5, 110.3, 97.7, 49.2, 44.4, 31.7, 28.7, 27.2, 27.0, 22.9, 14.1; UV–vis (CH_2Cl_2): λ_{max} (ε) = 573 nm (312000 M^{-1} cm^{-1}); HRMS (ESI) *m/z*: $[M]^+$ calcd for $C_{48}H_{52}N_2O_4$, 720.3922; found, 720.3926; Anal. calcd for $C_{48}H_{52}N_2O_4$: C 79.97, H 7.27, N 3.89; found: C 79.67, H 7.33, N 3.85.

Synthesis of ***3***: This dye was synthesized using 4-(dibutylamino) benzaldehyde (**9**) as a starting material according to the same procedure described above for compound **1**. Yield: 460 mg (0.71 mmol, 36%), dark red solid; Mp. 346 °C; ^{1}H NMR (CD_2Cl_2, 400 MHz, δ): 8.55 (bs, 4H), 8.28–8.20 (m, 2H), 7.77 (s, 2H), 6.77 (d, J = 9.4 Hz, 4H), 3.45 (t, J = 7.9 Hz, 8H), 1.72–1.62 (m, 8H), 1.47–1.36 (m, 8H), 1.00 (t, J = 7.4 Hz, 12H); ^{13}C NMR (CD_2Cl_2, 151 MHz, δ): 190.5, 190.4, 188.6, 188.5, 153.8, 148.3, 147.4, 147.1, 145.1, 144.8, 139.3, 122.8, 122.2, 116.2, 116.1, 116.0, 112.1, 51.6, 29.9, 20.7, 14.1; UV–vis (CH_2Cl_2): λ_{max} (ε) = 579 nm (215000 M^{-1} cm^{-1}); HRMS (ESI) *m/z*: $[M]^+$ calcd for $C_{42}H_{48}N_2O_4$, 644.3609; found, 644.3609; Anal. calcd for $C_{42}H_{48}N_2O_4$: C 78.23, H 7.50, N 4.34; found: C 77.96, H 7.67, N 4.46.

Synthesis of Reference ***5***: This dye was synthesized from (*E*)-2-(1-hexyl-3,3-dimethylindolin-2-ylidene)acetaldehyde (**8**) and indane-1,3-dione according to the procedure described in the literature[22] for a similar compound. The product was purified by successive column chromatography (silica gel) with dichloromethane/methanol (100:1) and toluene/ethyl acetate (9:1). Yield: 520 mg (1.30 mmol, 38%), red solid; Mp. 197–198 °C; ^{1}H NMR (CD_2Cl_2, 400 MHz, δ): 8.12 (d, J = 14.1 Hz, 1H), 7.84–7.74 (m, 2H), 7.64–7.58 (m, 2H), 7.51 (d, J = 14.1 Hz, 1H), 7.35–7.30 (m, 2H), 7.18–7.12 (m, 1H), 6.97 (d, J = 8.0 Hz, 1H), 3.95 (t, J = 7.6 Hz, 2H), 1.89–1.80 (m, 2H), 1.73 (s, 6H), 1.52–1.29 (m, 6H), 0.89 (t, J = 7.0 Hz, 3H); ^{13}C NMR (CD_2Cl_2, 101 MHz, δ): 192.2, 191.2, 174.6, 143.1, 142.3, 142.0, 141.4, 140.7, 133.7, 133.4, 128.6, 124.1, 122.4, 121.8, 121.4, 117.1, 110.0, 96.8, 49.0, 44.3, 31.9, 29.0, 27.19, 27.16, 23.0, 14.1; UV–vis (CH_2Cl_2): λ_{max} (ε) = 497 nm (114000 M^{-1} cm^{-1}); HRMS (ESI) *m/z*: $[M]^+$ calcd for $C_{27}H_{29}NO_2$, 399.2193; found, 399.2189; Anal. calcd for $C_{27}H_{29}NO_2$: C 81.17, H 7.32, N 3.51; found: C 81.47, H 7.59, N 3.53.

Optical Spectroscopy: For all spectroscopic measurements, spectroscopic grade solvents (Uvasol) from Merck (Hohenbrunn, Germany) were used. UV–vis spectra of the synthesized compounds were recorded on Perkin Elmer UV–vis spectrometers Lamda 950, Lamda 35, or Lamda 40P. Fluorescence spectra were recorded with a PTI QM-4/2003 instrument under ambient conditions. The fluorescence quantum yields were determined by optical dilution method[34] (*Abs* < 0.05) using *N*,*N*′-di(2,6-diisopropylphenyl)-1,6,7,12-tetraphenoxyperylene-3,4:9,10-tetracarboxylic acid bisimide[24] (Φ_{em} = 0.96 in $CHCl_3$) for all D–A–D dyes or *N*,*N*′-di(2,6-diisopropylphenyl)-perylene-3,4:9,10-tetracarboxylic acid bisimide[25] (Φ_{em} = 1 in $CHCl_3$) for D–A dyes as references. Lifetimes were determined with a PTI GL3330 nitrogen laser and a GL302 dye Laser. Evaluation of the fluorescence decay curves was performed with PTI Felix32 software.

Cyclic Voltammetry (CV): The cyclic voltammetry measurements were performed on a standard, commercial electrochemical analyzer (EC epsilon; BAS Instruments, UK) in a three electrode single-compartment cell in an argon atmosphere. Dichloromethane (HPLC grade) was dried

© 2014 WILEY-VCH Verlag GmbH & Co. KGaA, Weinheim

over calcium hydride in an argon atmosphere and degassed prior to use. The supporting electrolyte NBu_4PF_6 was synthesized according to literature,[35] recrystallized from ethanol/water, and dried in high vacuum. The measurements were carried out under exclusion of air and moisture at a concentration of approximately 2.5×10^{-4} M with ferrocene as an internal standard for the calibration of the potential. Working electrode: Pt disc; reference electrode: Ag/AgCl; auxiliary electrode: Pt wire.

Device Fabrication and Characterization: All solar cell devices were fabricated on commercial indium-tin oxide (ITO) coated glass. The ITO was etched with $FeCl_3$/HCl solution and subsequently cleaned using chloroform, acetone, mucasol detergent and de-ionized water in ultrasonic bath. As next, the ITO substrates were exposed to ozone for 10 minutes and immediately coated with poly(3,4-ethylene dioxythiophene):poly(styrene sulfonate) (PEDOT:PSS) (Clevios Al 4083, Heraeus; ca. 35 nm). Afterwards, the samples were heat treated for 2 minutes at 110 °C to remove residual water and transferred into a N_2 glove box for the fabrication of devices and measurements. For devices with MoO_3 as hole collecting contact, 15 nm of MoO_3 (Alfa Aesar, 99.95%) were deposited on the precleaned ITO substrates by thermal evaporation. The dyes, $PC_{61}BM$ (≥99.5%, Nano-C) and $PC_{71}BM$ (≥99%, Nano-C) were separately dissolved (10 mg mL^{-1} each) in chloroform (≥99.8%, Sigma Aldrich). The solutions were mixed with specific volumes to give the desired donor:acceptor weight ratio. Film thickness was adjusted by regulating the rotation speed for spin-coating. The substrates were transferred to a high-vacuum chamber where the top electrodes were evaporated. Here, a 4 nm thick Ca (99.5%, Alfa Aesar) layer and subsequently a 150 nm thick Ag (99.9%, Alfa Aesar) layer were deposited through a mask. On each substrate, seven solar cells with an active area of 0.0785 cm^2 are obtained.

The *J–V* characteristics of the solar cells were measured using a Keithley 2425 source measurement unit with simulated AM1.5 sun light provided by a filtered Xe lamp. The intensity of 100 mW cm^{-2} of the light was determined by using a calibrated inorganic solar cell from the Fraunhofer Institute for solar research (ISE) in Freiburg, Germany and a reference P3HT:PCBM cell measured by the same institute. No spectral mismatch factor was included in the calculation of the efficiency. The *EQE* measurements were performed using an Oriel QE/IPCE Measurement Kit. *EQE* spectra have been corrected for intensity dependence according to a method described by Janssen et al.[36] J_{SC} values calculated by integrating the product of *EQE* spectra and AM1.5 spectrum were found to match measured J_{SC} values within 5%. Layer thicknesses were determined with a Dektak surface profiler (Veeco).

Supporting Information

Supporting Information is available from the Wiley Online Library or from the author.

Acknowledgements

Financial support by the BMBF within the LOTsE project is gratefully acknowledged. We thank Dr. Peter Erk and Dr. Helmut Reichelt (BASF SE, Ludwigshafen) for helpful discussions.

Received: February 10, 2014
Revised: March 7, 2014
Published online: May 2, 2014

[1] For reviews, see: a) M. C. Scharber, D. Mühlbacher, M. Koppe, P. Denk, C. Waldauf, A. J. Heeger, C. J. Brabec, *Adv. Mater.* **2006**, *18*, 789; b) B. Kippelen, J.-L. Brédas, *Energy Environ. Sci.* **2009**, *2*, 251; c) P. M. Beaujuge, J. M. J. Fréchet, *J. Am. Chem. Soc.* **2011**, *133*, 20009; d) Z. B. Henson, K. Müllen, G. C. Bazan, *Nature Chem.* **2012**, *4*, 699.

[2] For reviews on polymer-based OSC, see: a) Y. Cheng, S. Yang, C. S. Hsu, *Chem. Rev.* **2009**, *109*, 5868; b) H. Zhou, L. Yang, W. You, *Macromolecules* **2012**, *45*, 607.

[3] M. Hiramoto, H. Fujiwara, M. Yokoyama, *Appl. Phys. Lett.* **1991**, *58*, 1062.

[4] a) Z. He, C. Zhong, S. Su, M. Xu, H. Wu, Y. Cao, *Nat. Photon.* **2012**, *6*, 591; b) S. Liu, K. Zhang, J. Lu, J. Zhang, H.-L. Yip, F. Huang, Y. Cao, *J. Am. Chem. Soc.* **2013**, *135*, 15326; c) S.-H. Liao, H.-J. Jhuo, Y.-S. Cheng, S.-A. Chen, *Adv. Mater.* **2013**, *25*, 4766.

[5] For reviews on small molecule-based OSC, see: a) J. Roncali, *Acc. Chem. Res.* **2009**, *42*, 1719; b) Y. Li, Q. Guo, Z. Li, J. Pei, W. Tian, *Energy Environ. Sci.* **2010**, *3*, 1427; c) B. Walker, C. Kim, T. Q. Nguyen, *Chem. Mater.* **2011**, *23*, 470; d) Y. Lin, Y. Li, X. Zhan, *Chem. Soc. Rev.* **2012**, *41*, 4245; e) A. Mishra, P. Bäuerle, *Angew. Chem.* **2012**, *124*, 2060; *Angew. Chem. Int. Ed.* **2012**, *51*, 2020; f) Y. Chen, X. Wan, G. Long, *Acc. Chem. Res.* **2013**, *46*, 2645.

[6] a) J. Mei, K. R. Graham, R. Stalder, J. R. Reynolds, *Org. Lett.* **2010**, *12*, 660; b) S. Steinberger, A. Mishra, E. Reinold, J. Levichkov, C. Uhrich, M. Pfeiffer, P. Bäuerle, *Chem. Commun.* **2011**, *47*, 1982; c) R. Fitzner, E. Mena-Osteritz, A. Mishra, G. Schulz, E. Reinold, M. Weil, C. Körner, H. Ziehlke, C. Elschner, K. Leo, M. Riede, M. Pfeiffer, C. Uhrich, P. Bäuerle, *J. Am. Chem. Soc.* **2012**, *134*, 11064; d) Z. Li, G. He, X. Wan, Y. Liu, J. Zhou, G. Long, Y. Zuo, M. Zhang, Y. Chen, *Adv. Energy Mater.* **2012**, *2*, 74; e) J. Zhou, X. Wan, Y. Liu, Y. Zuo, Z. Li, G. He, G. Long, W. Ni, C. Li, X. Su, Y. Chen, *J. Am. Chem. Soc.* **2012**, *134*, 16345.

[7] a) B. Walker, A. B. Tamayo, X. D. Dang, P. Zalar, J. H. Seo, A. Garcia, M. Tantiwiwat, T. Q. Nguyen, *Adv. Funct. Mater.* **2009**, *19*, 3063; b) M. Velusamy, J.-H. Huang, Y.-C. Hsu, H.-H. Chou, K.-C. Ho, P.-L. Wu, W.-H. Chang, J. T. Lin, C.-W. Chu, *Org. Lett.* **2009**, *11*, 4898; c) A. Leliège, P. Blanchard, T. Rousseau, J. Roncali, *Org. Lett.* **2011**, *13*, 3098.

[8] S. Steinberger, A. Mishra, E. Reinold, C. M. Müller, C. Uhrich, M. Pfeiffer, P. Bäuerle, *Org. Lett.* **2011**, *13*, 90.

[9] a) T. S. van der Poll, J. A. Love, T.-Q. Nguyen, G. C. Bazan, *Adv. Mater.* **2012**, *24*, 3646; b) C. J. Takacs, Y. Sun, G. C. Welch, L. A. Perez, X. Liu, W. Wen, G. C. Bazan, A. J. Heeger, *J. Am. Chem. Soc.* **2012**, *134*, 16597; c) Z. B. Henson, G. C. Welch, T. van der Poll, G. C. Bazan, *J. Am. Chem. Soc.* **2012**, *134*, 3766.

[10] a) V. Steinmann, N. M. Kronenberg, M. R. Lenze, S. M. Graf, D. Hertel, K. Meerholz, H. Bürckstümmer, E. V. Tulyakova, F. Würthner, *Adv. Energy Mater.* **2011**, *1*, 888; b) H. Bürckstümmer, E. V. Tulyakova, M. Deppisch, M. R. Lenze, N. M. Kronenberg, M. Gsänger, M. Stolte, K. Meerholz, F. Würthner, *Angew. Chem.* **2011**, *123*, 11832; *Angew. Chem. Int. Ed.* **2011**, *50*, 11628.

[11] a) Y.-H. Chen, L.-Y. Lin, C.-W. Lu, F. Lin, Z.-Y. Huang, H.-W. Lin, P.-H. Wang, Y.-H. Liu, K.-T. Wong, J. Wen, D. J. Miller, S. B. Darling, *J. Am. Chem. Soc.* **2012**, *134*, 13616; b) S.-W. Chiu, L.-Y. Lin, H.-W. Lin, Y.-H. Chen, Z.-Y. Huang, Y.-T. Lin, F. Lin, Y.-H. Liu, K.-T. Wong, *Chem. Commun.* **2012**, *48*, 1857.

[12] H. Shang, H. Fan, Y. Liu, W. Hu, Y. Li, X. Zhan, *Adv. Mater.* **2011**, *23*, 1554.

[13] a) T. Rousseau, A. Cravino, E. Ripaud, P. Leriche, S. Rihn, A. De Nicola, R. Ziessel, J. Roncali, *Chem. Commun.* **2010**, *46*, 5082; b) T. Bura, N. Leclerc, S. Fall, P. Lévêque, T. Heiser, P. Retailleau, S. Rihn, A. Mirloup, R. Ziessel, *J. Am. Chem. Soc.* **2012**, *134*, 17404.

[14] a) F. Silvestri, M. D. Irwin, L. Beverina, A. Facchetti, G. A. Pagani, T. J. Marks, *J. Am. Chem. Soc.* **2008**, *130*, 17640; b) U. Mayerhöffer, K. Deing, K. Gruss, H. Braunschweig, K. Meerholz, F. Würthner, *Angew. Chem.* **2009**, *121*, 8934; *Angew. Chem. Int. Ed.* **2009**, *48*, 8776; c) G. Wei, S. Wang, K. Sun, M. E. Thompson, S. R. Forrest, *Adv. Energy Mater.* **2011**, *1*, 184.

[15] F. Würthner, R. Wortmann, K. Meerholz, *ChemPhysChem* **2002**, *3*, 17.

© 2014 WILEY-VCH Verlag GmbH & Co. KGaA, Weinheim

[16] a) A. Dieckmann, H. Bässler, P. M. Borsenberger, *J. Chem. Phys.* **1993**, *99*, 8136; b) D. Hertel, H. Bässler, *ChemPhysChem* **2008**, *9*, 666.
[17] F. Würthner, S. Yao, T. Debaerdemaeker, R. Wortmann, *J. Am. Chem. Soc.* **2002**, *124*, 9431.
[18] F. Würthner, K. Meerholz, *Chem. Eur. J.* **2010**, *16*, 9366.
[19] P. Krief, J. Y. Becker, A. Ellern, V. Khodorkovsky, O. Neilands, L. Shapiro, *Synthesis* **2004**, *15*, 2509.
[20] N. M. Kronenberg, M. Deppisch, F. Würthner, H. W. A. Lademann, K. Deing, K. Meerholz, *Chem. Commun.* **2008**, 6489.
[21] M. Hauck, M. Stolte, J. Schönhaber, H.-G. Kuball, T. J. J. Müller, *Chem. Eur. J.* **2011**, *17*, 9984.
[22] S. Krause, M. Stolte, F. Würthner, N. Koch, *J. Phys. Chem. C* **2013**, *117*, 19031.
[23] H. Zollinger, *Color Chemistry*, 3rd ed., Wiley-VCH, Weinheim **2003**.
[24] R. Gvishi, R. Reisfeld, Z. Burshtein, *Chem. Phys. Lett.* **1993**, *213*, 338.
[25] G. Seybold, G. Wagenblast, *Dyes Pigm.* **1989**, *11*, 303.
[26] K. Rurack, *Springer Ser. Fluoresc.* **2008**, *5*, 101.
[27] S. Roquet, A. Cravino, P. Leriche, O. Alévêque, P. Frère, J. Roncali, *J. Am. Chem. Soc.* **2006**, *128*, 3459.
[28] N. P. Redmore, I. V. Rubtsov, M. J. Therien, *J. Am. Chem. Soc.* **2003**, *125*, 8769.
[29] a) A. A. Ishchenko, *Russ. Chem. Rev.* **1991**, *60*, 865; b) A. A. Ishchenko, A. V. Kulinich, S. L. Bondarev, V. N. Knyukshto, *J. Phys. Chem. A* **2007**, *111*, 13629; c) V. Karunakaran, J. L. Pérez Lustres, L. Zhao, N. P. Ernsting, O. Seitz, *J. Am. Chem. Soc.* **2006**, *128*, 2954; d) J. Conyard, M. Kondo, I. A. Heisler, G. Jones, A. Baldridge, L. M. Tolbert, K. M. Solntsev, S. R. Meech, *J. Phys. Chem. B* **2011**, *115*, 1571.
[30] C. Reichardt, *Solvents and Solvent Effects in Organic Chemistry*, 3rd ed., Wiley-VCH, Weinheim **2003**.
[31] The FMO energies were calculated from the determined half-wave or peak potentials applying the equations $E_{HOMO} = -5.15$ eV $-E_{ox}^{1}$ and $E_{LUMO} = -5.15$ eV $-E_{red}^{1}$.
[32] Y. He, Y. Li, *Phys. Chem. Chem. Phys.* **2011**, *13*, 1970.
[33] J. Meyer, S. Hamwi, M. Kröger, W. Kowalsky, T. Riedl, A. Kahn, *Adv. Mater.* **2012**, *24*, 5408.
[34] J. R. Lakowicz, *Principles of Fluorescence Spectroscopy*, Kluwer Academic/Plenum Publishers, New York **1999**.
[35] A. J. Fry, in *Laboratory Techniques in Electroanalytical Chemistry*, 2nd Ed. (Eds: P. T. Kissinger, W. R. Heineman), Marcel Dekker Ltd, New York **1996**, p. 481.
[36] D. J. Wehenkel, K. H. Hendriks, M. M. Wienk, R. A. J. Janssen, *Organic Electronics* **2012**, *13*, 3284.

© 2014 WILEY-VCH Verlag GmbH & Co. KGaA, Weinheim